Journal of Nanobiotechnology

RESEARCH

Open Access

Photoimmunotherapy using indocyanine green-loaded *Codium fragile* polysaccharide and chitosan nanoparticles suppresses tumor growth and metastasis

Dayoung Ryu[1†], Hae-Bin Park[2†], Eun-Koung An[2], So-Jung Kim[2], Da young Kim[2], Daeun Lim[2], Juyoung Hwang[3], Minseok Kwak[3], Wonpil Im[4], Ja-Hyoung Ryu[5], SangGuan You[6*], Peter C. W. Lee[1*] and Jun-O Jin[2*]

Abstract

Metastasis and recurrence are the main challenges in cancer treatment. Among various therapeutic approaches, immunotherapy holds promise for preventing metastasis and recurrence. In this study, we evaluated the efficacy of treating primary cancer and blocking metastasis and recurrence with photo-immunotherapeutic nanoparticles, which were synthesized using two types of charged polysaccharides. *Codium fragile* polysaccharide (CFP), which exhibits immune-stimulating properties and carries a negative charge, was combined with positively charged chitosan to synthesize nanoparticles. Additionally, indocyanine green (ICG), a photosensitizer, was loaded inside these particles and was referred to as chitosan-CFP-ICG (CC-ICG). Murine colon cancer cells (CT-26) internalized CC-ICG, and subsequent 808-nanometer laser irradiation promoted apoptotic/necrotic cell death. Moreover, intratumoral injection of CC-ICG, with 808-nanometer laser irradiation eliminated CT-26 tumors in mice. Rechallenged lung metastases of CT-26 cancer were inhibited by dendritic cell activation-mediated cytotoxic T lymphocyte stimulation in mice cured by CC-ICG. These results demonstrated that CC-ICG is a natural tumor therapeutic with the potential to treat primary tumors and suppress metastasis and recurrence.

Keywords *Codium fragile* polysaccharide, Chitosan, Nanoparticle, Photoimmunotherapy, Lung metastasis

[†]Dayoung Ryu and Hae-Bin Park contributed equally to this work.

*Correspondence:
SangGuan You
umyousg@gwnu.ac.kr
Peter C. W. Lee
pclee@amc.seoul.kr
Jun-O Jin
junojin@amc.seoul.kr
[1]Department of Biochemistry and Molecular Biology, Brain Korea 21 project, University of Ulsan College of Medicine, ASAN Medical Center, Seoul 05505, South Korea
[2]Department of Microbiology, Brain Korea 21 project, University of Ulsan College of Medicine, ASAN Medical Center, Seoul 05505, South Korea
[3]Department of Chemistry, Pukyong National University, Busan 48513, South Korea
[4]Departments of Biological Sciences, Lehigh University, Bethlehem, PA, USA
[5]Department of Chemistry, Ulsan National Institute of Science and Technology (UNIST), Ulsan 44919, South Korea
[6]Department of Marine Food Science and Technology, Gangneung-Wonju National University, 120 Gangneung Daehangno, Gangneung, Gangwon 210-702, South Korea

Introduction

Advancements in the life sciences and medical technologies have allowed for effective cancer treatments [1, 2]. However, many patients still experience cancer metastasis and recurrence [3, 4]. These phenomenon occur via complex mechanisms, often accompanied by high anticancer drug resistance [5, 6]. Anticancer treatments have been combined to prevent metastasis or recurrence; however, no promising results have been found.

Cancer immunotherapy is evolving rapidly [7, 8], offering minimal side effects compared to traditional chemotherapy [7]. Immunotherapy leverages immune cells of the body to eliminate tumors, with techniques such as immune checkpoint inhibitors, cancer vaccines, and chimeric antigen receptor T cell treatments now in clinical use [9]. These treatments work by activating cytotoxic T lymphocytes (CTL) [9], which selectively induce cancer cell death with minimal impact on normal cells [7, 9]. Therefore, effective induction of CTL activity blocks cancer metastasis or recurrence, and many studies are being conducted for this purpose.

CTL activity is triggered by dendritic cells (DC) [10] that capture invading antigens and present specific proteins to T cells [10], promoting their differentiation and proliferation [10]. However, cancer antigens are proteins derived from patient cells and limit the activity of DCs [11]. In cases where DC activity cannot be sufficiently induced against antigens, vaccines are manufactured by adding adjuvants, which are immune activators [10–12]. Adjuvants enhance antigen-specific immune activity by inducing DC stimulation, thereby helping to induce the efficient cytotoxicity of CTLs against antigen-expressing cells [12]. Thus, cancer immunotherapy using appropriate adjuvants is necessary, as cancer antigens are not immunogenic.

Natural polysaccharides exhibit various physiological activities, including anticancer, anti-inflammatory, and immune stimulatory activities [13, 14]. *Codium fragile* (*C. fragile*) is consumed as food in Asia, and *C. fragile* polysaccharide (CFP) confers its anticancer effects via activation of DCs [15, 16], natural killer cells, and CTLs in both mice and humans [15–17]. Chitosan is a polysaccharide extracted from the shells of crustaceans, such as shrimp, and is used in pharmaceutical and biomedical fields [18]. Chitosan has many advantages, including low immune response induction, excellent biocompatibility, a high degree of biodegradability, and natural abundance [18, 19]. It functions as a drug carrier; however, because it is positively charged, chitosan is used as a drug carrier by forming a nanostructure with a negatively charged material [20].

Photothermal therapy (PTT) is a tumor treatment [21] that employs laser irradiation to generate localized heat. This method offers the advantage of minimizing damage to surrounding tissues [21]. For this treatment, a photosensitizer that converts the light energy of a near-infrared (NIR) laser into heat energy is required [22]. Although various photosensitizers are being developed, indocyanine green (ICG) is actively used because of its stability in the body [22]. Recent advances in nanoparticles technology have enhanced the efficacy of PTT by enabling targeted tumor irradiation using NIR-loaded nanoparticles, such as ICG [23, 24].

In this study, we synthesized nanostructures by combining CFP, which has a negative charge and functions as an immune stimulator, with chitosan, which has a positive charge. ICG was loaded inside the nanoparticles to make them suitable for photoimmunotherapy against cancer; these were named chitosan-CFP-ICG (CC-ICG) nanoparticles. We hypothesized that CC-ICG-mediated PTT would treat primary tumors by blocking metastasis and recurrence through its immunotherapeutic ability (Scheme 1).

Methods

CFP purification

Polysaccharides from *C. fragile* were extracted following the procedure described by Tabarsa et al. [25]. Briefly, dried samples were immersed in 90% ethanol, followed by hot water extraction at 65 °C once the ethanol had completely evaporated. The water-soluble crude polysaccharides were precipitated using ethanol treatment. Additionally, the Sevag technique was employed to remove the unbound proteins from the polysaccharides. To further enhance the purification, the sample was loaded onto a diethylaminoethyl Sepharose fast flow column (17–0709-01, GE Healthcare Bio-Science AB, Uppsala, Sweden). Three active fractions, CFP-F1, CFP-F2, and CFP-F3 were collected. Among these fractions, CFP-F2 demonstrated an excellent immune response and was therefore selected for further studies [15–17, 25, 26].

CC-ICG synthesis

CC-ICG nanoparticles were synthesized using ultrasonication at room temperature. CFP was dissolved in distilled water, and chitosan (Daejung, Korea) was dissolved in a 1% (v/v) acetic acid solution. The two polysaccharides were mixed in the following ratios: 1:1, 1:2, and 1:3. Ultrasonication was then performed to form nanoparticles through material entanglement on ice under the following conditions: pulse-on 3 s, pulse-off 7 s, for a total of 3 min at 40% amplitude. The total volume of the mixture was fixed at 6 mL, and 2 mg of ICG was added (Tokyo Chemical Industry, Tokyo, Japan). The nanoparticles were harvested using centrifugation at 6200 × g for 10 min, and the pellet was resuspended in distilled water.

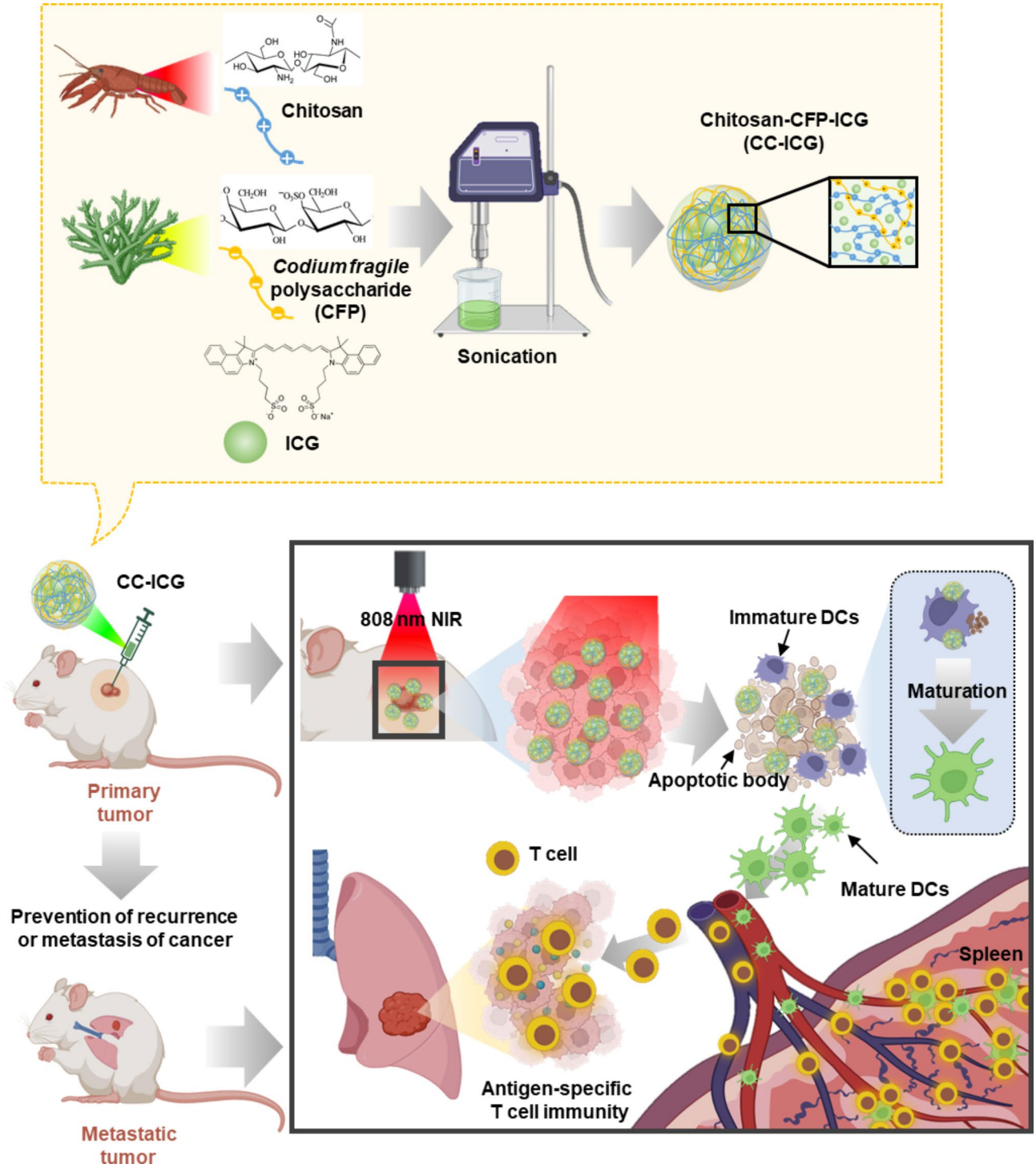

Scheme 1 Induction of complete primary tumor remission and inhibition of lung cancer metastasis or recurrence by CC-ICG-mediated photoimmunotherapy. CFP, *Codium fragile* polysaccharide; ICG, indocyanine green; CC-ICG, chitosan-CFP-ICG; NIR, near-infrared; DC, dendritic cell

CC-ICG characterization

CFP, chitosan, and chitosan-CFP (CC) levels were measured using a Fourier Transform Infrared Spectrometer (JASCO, FT-4100, Tokyo, Japan). The zeta potential and nanoparticle size were determined using a Dynamic Light Scattering Particle Analyzer (Litesizer DLS 500; Anton Paar, Graz, Austria). Transmission electron microscopy (TEM) images were obtained using an H-7600 transmission electron microscope (Hitachi, Tokyo, Japan). The encapsulated ICG amount was quantified using a UV–vis

spectrophotometer (Cary 100 Bio; Varian, Palo Alto, CA, USA). PTT was performed using a fiber-coupled continuous-wave diode laser (808 nm; Changchun New Industries Optoelectronics Technology Co., Ltd., Jilin, China), and temperature changes and thermal images were obtained using a MobIR Air Mobile Phone Thermal Imaging Camera (ZIYOUHU, China).

Cell line and cell culture

The murine colon carcinoma cell line CT-26 (ATCC, CRL-2638; Korean Cell Line Bank, Seoul, Korea) was cultured in RPMI-1640 medium with 1% penicillin/streptomycin and 10% fetal bovine serum (FBS). CT-26WT-iRFP-Neo cells (CT-26-iRFP; Imanis Life Sciences, CL091, Rochester, USA) were cultured in an RPMI-1640 medium with 1% penicillin/streptomycin, 10% FBS, and 0.4 mg/mL G418. Both cell lines were maintained in a 5% CO_2 incubator at 37 °C.

Annexin V/DAPI staining

CT-26 cells (1×10^5 cells/well) were seeded in 24-well plates (SPL Life Sciences Co., Ltd., Korea) and treated with phosphate-buffered saline (PBS), chitosan, CFP, CC, and CC-ICG. One hour after treatment, cells were irradiated with an NIR laser at 1, 1.5, and 2 W/cm^2 for 5 min. Twenty-four hours post-irradiation, cells were harvested and stained with annexin V- fluorescein isothiocyanate (FITC) (BioLegend, San Diego, CA, USA) and 4′,6-diamidino-2-phenylindole (DAPI; Sigma-Aldrich) at room temperature in the dark for 15 min. The apoptotic/necrotic cells were analyzed using flow cytometry (NovoCyte; ACEA Biosciences, San Diego, CA, USA).

Mice

Five- to six-week-old female C57BL/6 and BALB/c mice (20±0.2 g) were purchased from Orient Bio (Gyeonggi, Korea). Mice were raised in pathogen-free conditions at the Laboratory Animal Center of Asan Medical Center. All animal experiments were approved and conducted according to the guidelines of the National Research Council's Guide for the Care and Use of Laboratory Animals and the Institutional Animal Care and Use Committee at Asan Medical Center (Protocol number: 2023-20-260).

Antibodies

Fluorescently labeled Brilliant Violet 785™ anti-mouse cluster of differentiation (CD)11c, FITC anti-mouse CD3, FITC anti-mouse CD90.1, FITC anti-mouse Gr-1, FITC anti-mouse CD49b, FITC anti-mouse TER-119, allophycocyanin (APC) anti-mouse CD40, Brilliant Violet 605™ anti-mouse CD80, phycoerythrin (PE)/Cyanine7 anti-mouse CD86, peridinin-chlorophyll-protein (PerCP) anti-mouse I-A/I-E, PerCP/Cyanine5.5 anti-mouse H-2 Kb, PE/Cyanine7 anti-mouse T cell receptor (TCR)-β, PerCP5.5 anti-mouse CD4, Brilliant Violet 785™ anti-mouse CD8, and APC anti-mouse CD44 were purchased from BioLegend (San Diego, CA, USA).

Generation of bone marrow-derived dendrite cells (BMDC)

Bone marrow (BM) was harvested from the hind limbs of six-week-old C57BL/6 mice. The collected BM was suspended in red blood cell lysis buffer (Thermo Fisher, Waltham, MA, USA) and washed with PBS. BM cells (1×10^6 cells/mL of culture medium) were seeded in 24-well plates. The cells were incubated with 100 ng/mL of recombinant murine interleukin-4 and 100 ng/mL of recombinant granulocyte marcrophage colony stimulating factor. The differentiation of BMDCs was confirmed by CD11c expression on day 6 of culture using flow cytometry (NovoCyte, ACEA Biosciences, Inc.).

Analysis of BMDC activation

CT-26 cells (1×10^5 cells/mL) were seeded in 24-well plates and treated with PBS, chitosan, CFP, CC, and CC-ICG, followed by irradiated with an NIR laser for 5 min at 1.5 W/cm^2. Twenty-four hours after treatment, the culture medium was collected. On day 6, the BMDC culture medium was removed and replaced with the collected CT-26 culture medium. Twenty-four hours after incubation, BMDC morphology was observed using a microscope (EVOS M5000; Thermo fisher), and co-stimulatory and major histocompatibility complex (MHC) molecule expression were analyzed using flow cytometry (ACEA Biosciences Inc.)

Analysis of splenic DC activation

To analyze splenic DC activation, C57BL/6 mice were injected intravenously (*i.v.*) with PBS, chitosan, CFP, CC, and CC-ICG. Six hours post-injection, the mice were sacrificed, and their spleens were harvested. The spleens were sectioned into small pieces using curved scissors and digested with collagenase IV and DNase-containing culture medium at 37 °C for 20 min. Aggregated and undigested tissues were removed using a 100-nm nylon mesh and washed with PBS. The pellet was resuspended in 5 mL of Histopaque-1077 (Sigma-Aldrich) and layered with 5 mL of fresh Histopaque-1077. FBS was then added to the upper layer of the cell suspension. The cells were centrifuged at 600 × g for 10 min without a break. The fraction that was denser than 1.077 g/cm^3 was harvested as leukocytes. The splenocytes were then stained with lineage and DC activation markers, as shown in previous studies [12, 27, 28]. The stained cells were analyzed using flow cytometry (NovoCyte, ACEA Biosciences, Inc.).

PTT of CT-26 tumor

CT-26 cells (5×10^5/100 μL of PBS) were subcutaneously injected into BALB/c mice. On day 7, the mice were randomly divided into five groups: PBS, chitosan, CFP, CC, and CC-ICG. The aforementioned compounds were injected intratumorally and were then irradiated with an NIR laser at 1.5 W/cm^2 for 5 min. Temperature changes and thermal images were obtained using a MobIR Air Mobile Phone Thermal Imaging Camera (ZIYOUHU, China). Tumor growth and survival rates were monitored.

Rechallenge of lung metastatic CT-26 cancer

For the rechallenge of lung metastatic CT-26 cancer, on day 38 after primary tumor inoculation, mice that were cured by CC-ICG and laser irradiation were *i.v.*-injected with CT-26-iRFP cells (5×10^5 cells/100 μL of PBS). The PBS-, chitosan-, CFP-, and CC-treated mice were also inoculated *i.v.* with CT-26-iRFP cells as control groups for the rechallenge. The survival of the mice was monitored for 30 days post-injection (day 62 of the primary CT-26 challenge). On days 7, 10, and 14 after the rechallenge of lung metastatic CT-26 cancer, near-infrared fluorescent protein (iRFP) fluorescence was imaged using the Xenogen In Vivo Imaging System 200 BLI system (Caliper Life Sciences). Survival rates of mice were monitored for 20 days after the rechallenge of 4T1-iRFP. The detailed schedule of tumor challenge is shown in Fig. S8.

Hematoxylin and eosin (H&E) staining

On day 21 of the CT-26 rechallenge, mice were sacrificed, and 1 mL of 3.7% formaldehyde was injected intratracheally. The lungs were harvested and fixed with 3.7% formaldehyde at 4 °C overnight, dehydrated, and embedded in paraffin. The embedded lung tissue was sectioned into 5-μm thick slices and placed on glass slides. The sections were stained with H&E (Sigma-Aldrich), and images were obtained using an EVOS M5000 microscope (Thermo Fisher Scientific).

Analysis of memory T cells

Splenocytes were harvested on day 21 post-rechallenge of lung metastatic CT-26 cells. The splenocytes were stained with anti-CD8, anti-CD4, anti-TCR-β, and anti-CD44 for 20 min at 4 °C. Cells were washed with PBS and suspended in PBS containing DAPI (Sigma-Aldrich). The cells were analyzed using Novocyte (ACEA Biosciences, Inc.).

Live imaging for CTL activity

CD8 T cells were isolated from the splenocytes of CT-26 rechallenged mice using a CD8 T cell isolation kit (Miltenyi Biotec, Bergisch Gladbach, North Rhine-Westphalia, Germany). Isolated CD8 T cells (1×10^5) were cultured with CT-26-iRFP cells (1×10^4) in 24-well plates. Live images of CTL activity were obtained using a fluorescence microscope (EVOS M5000, Thermo Fisher Scientific) and live cell instruments (LCIbio, Gyeonggi-do, Korea) for 16 h.

Statistical analysis

Data are presented as the mean±standard error of the mean. One-way or two-way Tukey multiple comparison tests were used to analyze the dataset. Statistical significance was set at $p<0.05$.

Results

CC-ICG synthesis

Nanoparticles were synthesized using chitosan and CFP (Fig. 1A). Infrared spectroscopy was performed to substantiate the ionic interaction between CFP and chitosan during CC synthesis. Infrared spectroscopy reveals absorption bands associated with S=O asymmetric stretching and C-O-S stretching in CFP, which are present in CC [15]. Furthermore, the absorption band contributes to N-H bending, and a distinctive chitosan peak is also present in CC [29]. These findings indicated that CC was synthesized through electrostatic interactions between chitosan and CFP (Fig. 1B). The zeta potential of CC was measured at 25.4±1.2 mV (Fig. 1C and Table S1). TEM revealed that CC formed perfectly spherical nanoparticles with a size of 277.8±9.5 nm at a chitosan to CFP ration of 1:1 (Fig. 1D, E and Table S1). The ICG carrying rate of CC was 5.3±0.2%, which showed that 107.8 μg of ICG was carried in 4.5 mg of CC. Compared with that of CC, CC-ICG exhibited a slight increase in size (Fig. 1E and S1) and had a high absorbance at 808 nm (Fig. 1F). Therefore, these data indicated that CC-ICG was successfully synthesized.

CC-ICG-mediated PTT against CT-26 tumors

Under NIR laser irradiation for 5 min at 1.5 W/cm^2, the temperature of CC-ICG increased to 63.5±1.9 °C, whereas no temperature changes were observed with PBS, chitosan, CFP, or CC groups (Fig. 2A). In addition, the temperature of CC-ICG increased in a power-dependent manner due to NIR laser irradiation (Fig. 2B), and temperature increases were also concentration-dependent at a laser power of 1.5 W/cm^2 (Fig. 2C). Therefore, irradiation with NIR laser at 1.5 W/cm^2 for 5 min was set as the optimal parameters for PTT.

Considering that CC-ICG with NIR laser irradiation elevated the temperature, we next examined the effects of PTT on CT-26 cells, a colon cancer cell line. To confirm whether CC-ICG treatment enhanced phagocytosis compared to ICG treatment alone, we measured ICG fluorescence in CT-26 cells. CC-ICG-treated cells displayed strong ICG fluorescence, whereas free ICG showed

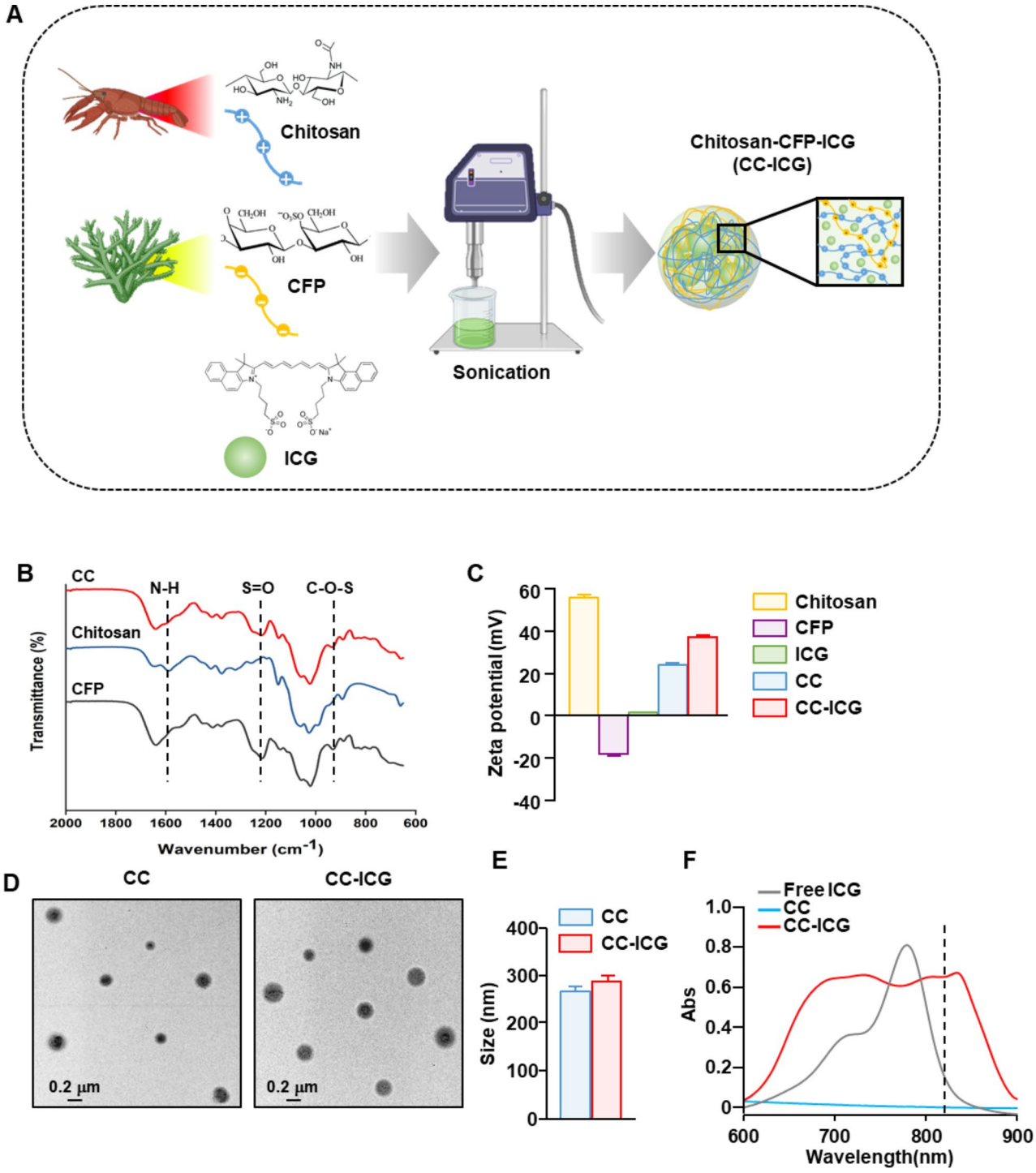

Fig. 1 Synthesis and characterization of chitosan-CFP-ICG nanoparticles **(A)** Schematic of CC-ICG synthesis. **(B)** Fourier transform infrared spectrometer images of chitosan, CFP, and CC. **(C)** Zeta potential of chitosan, CFP, ICG, Chito-ICG, CC, and CC-ICG. **(D)** Transmission electron microscope images of CC and CC-ICG. **(E)** Mean size of the particles. **(F)** The absorption spectra of ICG, CC, and CC-ICG. CFP, *Codium fragile* polysaccharide; ICG, indocyanine green; CC, chitosan-CFP; CC-ICG, chitosan-CFP-ICG; Chito, chitosan; Abs, absorbance

minimal fluorescence (Fig. 2D and S2). After irradiating CT-26 cells with an NIR laser for 5 min, CC-ICG treatment elevated the temperature to 63.7±0.5 °C, whereas the other treatments did not increase the temperature (Fig. S3). This temperature increase led to enhanced apoptotic/necrotic cell death in CC-ICG-treated CT-26 cells after NIR laser irradiation, whereas cell death was absent in the other control treatment groups (Fig. 2E).

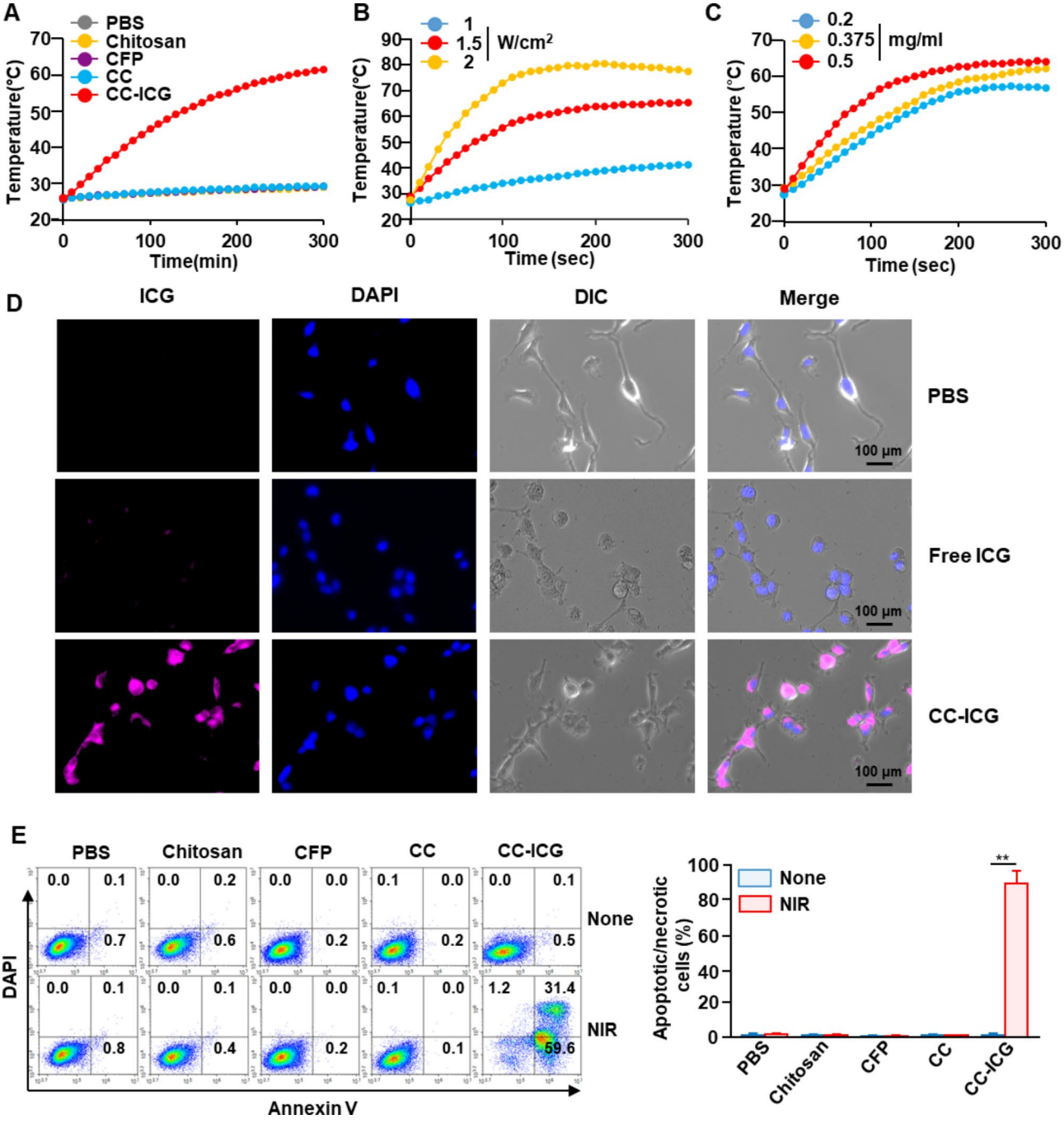

Fig. 2 CC-ICG with NIR irradiation induces apoptotic/necrotic cell death in CT-26 cells **(A)** Time-dependent heating curves of indicated reagent-treated culture medium irradiated by NIR laser at 1.5 W/cm^2 power for 5 min. **(B)** Temperatures changes depending on CC-ICG-treated culture medium and NIR laser power. **(C)** Dose-dependent temperature alterations by NIR laser irradiation at 1.5 W/cm^2 power for 5 min. **(D)** CT-26-iRFP cells are treated with PBS, 0.01 mg/mL ICG, and 0.5 mg/mL CC-ICG (chitosan: 0.245 mg, CFP: 0.245 mg, and ICG: 0.01 mg). One hour after treatment, ICG fluorescence is analyzed. Scale bar: 100 μm. **(E)** CT-26 cells were treated with the indicated reagents and irradiated with or without NIR laser at 1.5 W/cm^2 power for 5 min. Apoptotic/necrotic cell death is analyzed using Annexin V/DAPI staining (left panel). Mean percentage of apoptotic/necrotic cells is shown (right panel). Data are representative and averaged from six independent samples ($n = 6$, two-way ANOVA, mean ± SEM, $^{**}p < 0.01$). CFP, *Codium fragile* polysaccharide; CC, chitosan-CFP; ICG, indocyanine green; CC-ICG, chitosan-CFP-ICG; CT-26 cells, murine colon cancer cells; PBS, phosphate-buffered saline; NIR, near-infrared; DAPI, 4′,6-diamidino-2-phenylindole; ANOVA, analysis of variance; SEM, standard error mean

Therefore, these data indicate that CC-ICG can be used for PTT.

In vivo CC-ICG-mediated PTT against CT-26 tumor in mice

CC-ICG-mediated PTT was successful in CT-26 cells, we next examined whether CC-ICG-mediated PTT could eliminate CT-26 tumors in vivo. BALB/c mice with subcutaneous CT-26 tumors were intratumorally injected with PBS, chitosan, CFP, CC, and CC-ICG, and irradiated with an 808-nm laser at 1.5 W/cm^2 for 5 min. The surface temperature of the CT-26 tumor in CC-ICG-treated mice increased to 68.3±0.7 °C, whereas the temperature of the CT-26 tumors in the other control groups was unchanged (Fig. 3A and B). Three days post-PTT (10 days after tumor transplantation), tumors in the other control groups resumed growth, whereas only burn scars remained on the tumors in CC-ICG-treated mice (Fig. 3C upper panel). Thirteen days post-PTT (20 days after tumor transplantation), tumors CC-ICG-treated mice had completely disappeared, leaving only small burn scars, whereas the tumors in the other control groups grew remarkably (Fig. 3C low panel). In contrast,

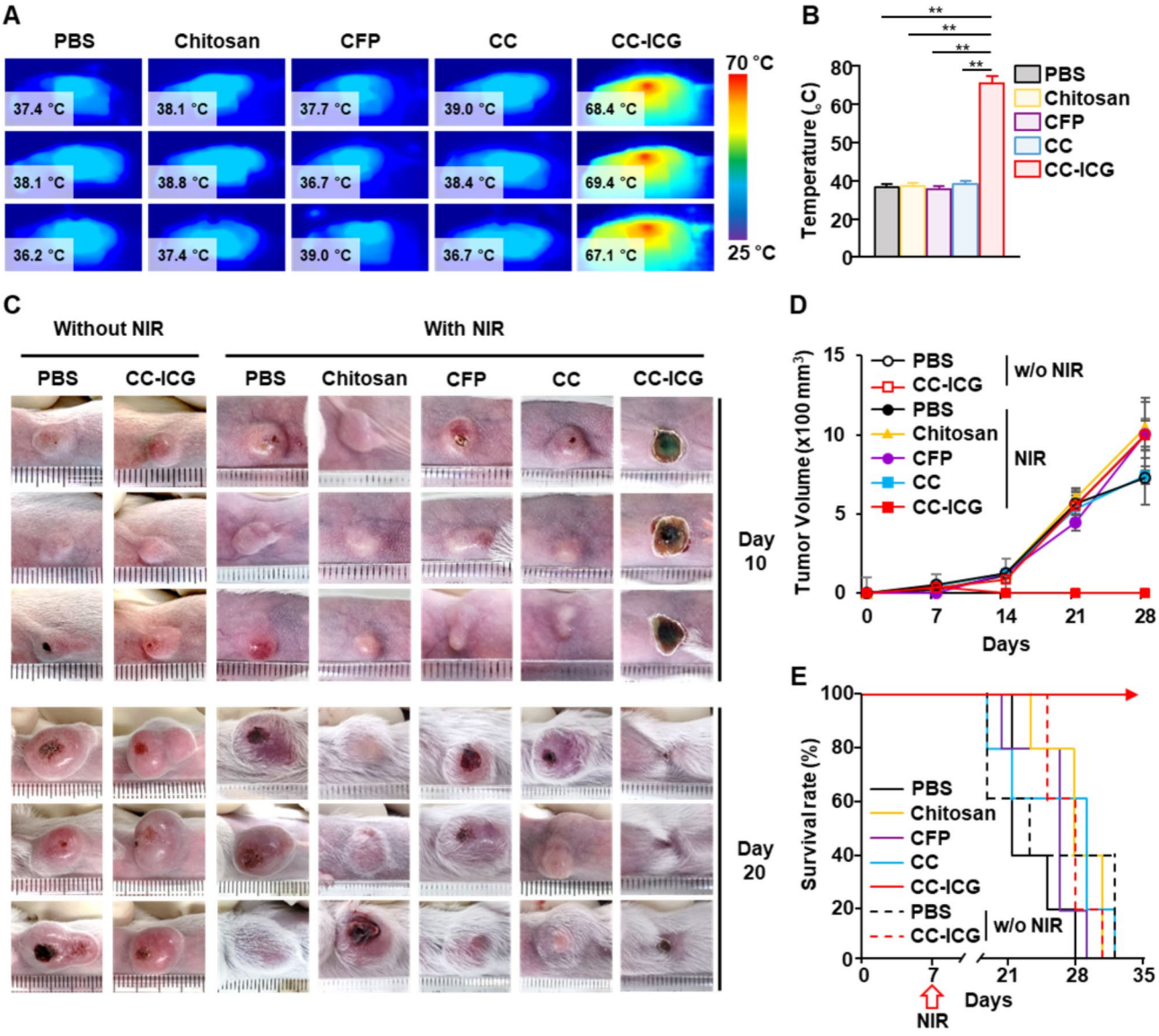

Fig. 3 CC-ICG-mediated PTT against CT-26 tumors in mice BALB/c mice are injected *s.c.* with 5×10^5 cells/100 μL of CT-26 cells. On day 7 after tumor inoculation, the mice are treated intratumorally with PBS, chitosan (12.5 mg/kg), CFP (12.5 mg/kg), CC (12.5 mg/kg chitosan and 12.5 mg/kg CFP), and CC-ICG (12.5 mg/kg chitosan, 12.5 mg/kg CFP, and 0.5 mg/kg ICG). The mice are immediately irradiated with an NIR laser at 1.5 W/cm^2 power for 5 min. **(A)** Thermal image of the tumor in mice after NIR laser irradiation. **(B)** Mean temperatures of the tumor after NIR laser irradiation ($n=6$, two-way ANOVA, mean ± SEM, $^{**}p<0.01$). **(C)** Tumor images in the mice at 10 and 20 days after CT-26 tumor inoculation. **(D)** Tumor growth curves ($n=6$). **(E)** Survival rate of mice ($n=5$). CFP, *Codium fragile* polysaccharide; CC, chitosan-CFP; ICG, indocyanine green; CC-ICG, chitosan-CFP-ICG; CT-26 cells, murine colon cancer cells; PBS, phosphate-buffered saline; NIR, near-infrared; *s.c.*, subcutaneously; w/o, without

injection of CC-ICG without NIR irradiation did not induce anti-tumor effects in the mice (Fig. 3C left panel). Moreover, while the tumors in the other control groups continued to grow, CC-ICG-mediated PTT exhibited complete tumor remission (Fig. 3D). In terms of survival rate, all mice treated with CC-ICG-mediated PTT survived, whereas all other control mice died within 31 days of tumor transplantation (Fig. 3E). These data demonstrated CC-ICG-mediated PTT can induce complete tumor remission in vivo.

Induction of DC activation by CC-ICG

We previously confirmed that CFP induces DC activation [15, 17, 30]. To evaluate if CC-ICG, which contains CFP, could similarly induce DC activation, BMDCs were treated with culture medium from CT-26 cells exposed to CC-ICG and controls, followed by NIR laser irradiation for PTT. After 24 h, the CC-ICG-treated culture medium transferred to BMDCs which induced dramatic changes in dendritic morphology and upregulated co-stimulators and MHC molecules in BMDCs, compared to that in control media treatments (Fig. S4). Next, we examined whether CFP-containing CC-ICG could induce splenic DC activation in mice after PTT (Fig. 4A). CT-26 tumor-bearing mice were treated with PBS, chitosan, CFP, CC, and CC-ICG and were irradiated with an NIR laser for 5 min. The frequency, population, and number of DCs substantially increased in the spleen of mice treated with CFP, CC, and CC-ICG, whereas no significant changes in the spleen DCs of PBS- and chitosan-treated mice were observed (Fig. 4B). In addition, the activity of co-stimulators and MHC molecules in splenic DCs were dramatically upregulated by CFP, CC, and CC-ICG treatment, whereas those in PBS- and chitosan-treated splenic DCs were not (Fig. 4C and D). Toxicity evaluation revealed that CC-ICG treatment in mice did not promote inflammation in the peripheral tissues or liver toxicity (Fig. S5 and S6). Moreover, CC-ICG in mice disappeared within 24 h in vivo and ex vivo (Fig. S7). Thus, these data suggest that CFP-containing CC and CC-ICG induces DC activation in the spleen without damaging peripheral tissues.

Prevention of lung metastatic CT-26-iRFP tumor growth in CC-ICG-mediated cured mice

Considering that CC-ICG-mediated PTT effectively treats primary CT-26 tumors and promotes splenic DC activation, we next examined whether the CC-ICG-cured mice could survive a rechallenge of lung metastatic CT-26-iRFP cancer. On day 32 after the primary tumor challenge, CT-26-iRFP cancer was re-administered intravenously to the mice whose primary CT-26 cancer had completely remitted (Fig. S8). Mice treated with PBS, chitosan, CFP, and CC all succumbed to metastatic tumor growth within 24 days after lung metastatic CT-26-iRFP administration (Fig. 5A). Mice whose primary CT-26 tumor was cured by CC-ICG survived for more than 30 days after re-administration of lung metastatic CT-26-iRFP (Fig. 5A). Moreover, in CC-ICG-cured mice, iRFP fluorescence was not observed in the lungs until 21 days after CT-26-iRFP re-administration, whereas iRFP fluorescence in other control groups was observed in the lungs 10 days after re-administration (Fig. 5B). On day 21 after the rechallenge, almost no infiltration of CT-26-iRFP cells was observed in the lungs of CC-ICG-cured mice, whereas a significant number of tumors had started growing in the lungs of mice from other control groups (Fig. 5C and S9). Histology data showed the infiltration of CT-26-iRFP cells into the lungs in the control groups, whereas it was hardly observed in CC-ICG-cured mice (Fig. 5D). These findings suggest that CC-ICG-cured mice were able to suppress the growth of lung metastatic cancer upon re-administration.

CC-ICG-induced T cell immunity contributes to protection against rechallenged CT-26 cancer

To identify the mechanism for suppressing the lung metastatic CT-26 growth upon re-administration in CC-ICG-cured mice, we evaluated the effect of CC-ICG on the induction of T cell immunity. Twenty-one days after re-administration of CT-26, splenic T cell activity was confirmed. T cells in the spleen were gated into cells expressing TCR-β among living leukocytes (Fig. 6A and S10A). The total number of splenic T cells, including CD4 and CD8 subsets, was significantly increased in CC-ICG-cured mice compared with those in other control group mice (Fig. 6A and S10B). Additionally, the proportion and population of memory CD4 and CD8 T cells expressing CD44 increased dramatically in mice treated with CC-ICG compared with those in mice from the other control groups (Fig. 6B and S11). We next co-cultured isolated CD8 and CT-26 cells to determine whether the T cells could exhibit cytotoxicity toward CT-26 cells (Fig. 6C). CD8 T cells from the spleen of CC-ICG-cured mice exhibited strong cytotoxicity towards CT-26-iRFP cells, penetrating the tumor cells (Fig. 6D and Video S5). In contrast, CD8 T cells isolated from the spleens of other control mice exhibited no substantial aggressiveness towards CT-26-iRFP cells (Fig. 6D and Video S1–4). In addition, CD8 T cells from CC-ICG-cured mice produced high levels of interferon-γ, tumor necrosis factor-α, and perforin during co-culture with CT-26-iRFP, whereas T cells from control group mice did not (Fig. 6E). Therefore, these data demonstrated that CD8 T cells from CC-ICG-cured mice exhibited cytotoxic ability against re-administered cancer cells.

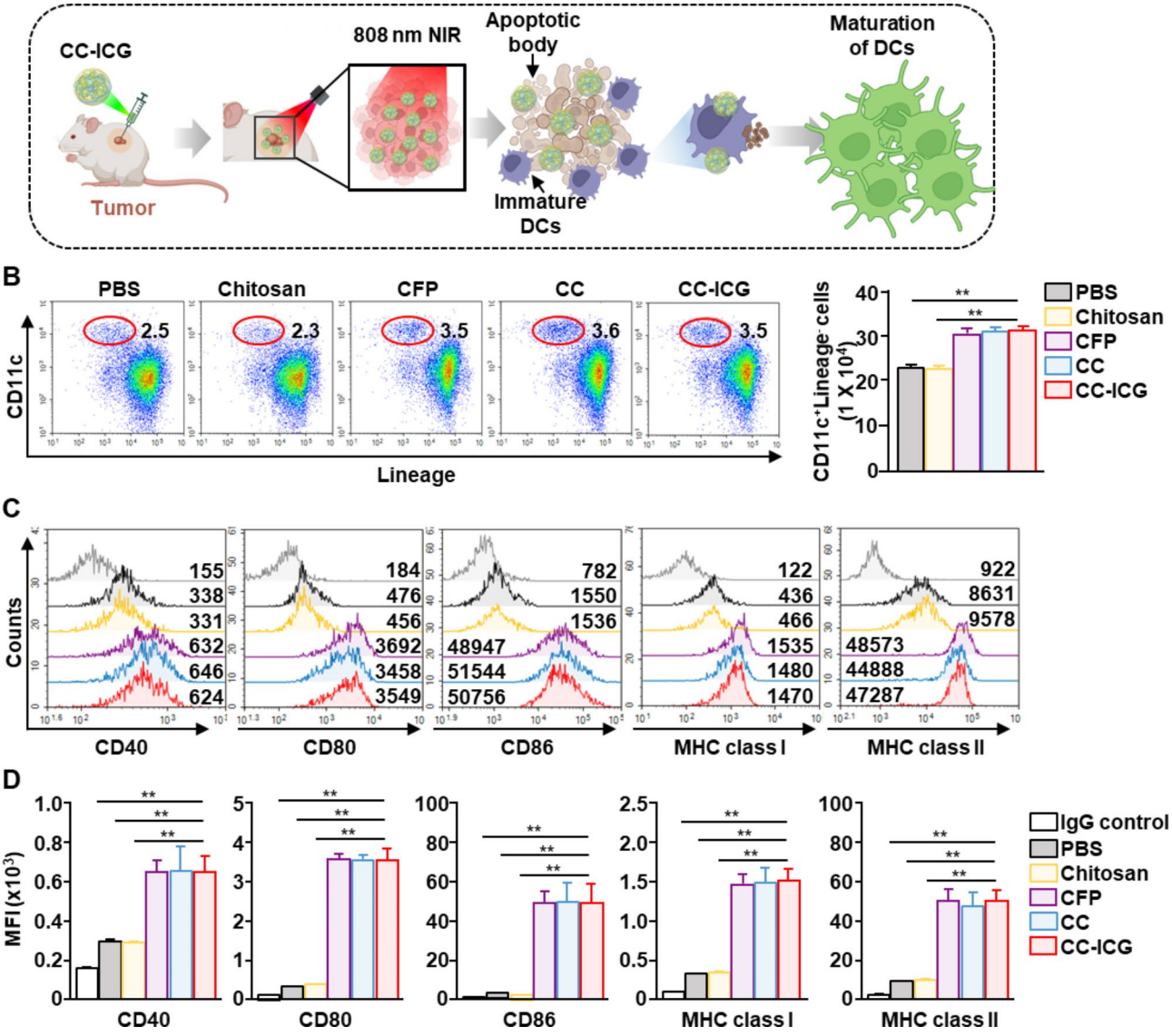

Fig. 4 CC-ICG-induced activation of splenic DCs CT-26 tumor-bearing mice are treated with PBS, chitosan, CFP, CC, and CC-ICG, and irradiated with an NIR laser. Six hours after injection, the mice are sacrificed, and the spleens are harvested. **(A)** Schematic illustration of the analysis strategy for splenic DCs. **(B)** Population and frequency of splenic DCs (left panel). Absolute number of splenic DCs (right panel). **(C)** Co-stimulator and MHC molecule expression in splenic DCs. **(D)** Mean fluorescence intensity (MFI) of the co-stimulator and MHC molecule population of splenic DCs. Data are representative and averaged from six independent samples ($n = 6$, two-way ANOVA, mean ± SEM, $^{**}p < 0.01$). CFP, *Codium fragile* polysaccharide; CC, chitosan-CFP; ICG, indocyanine green; CC-ICG, chitosan-CFP-ICG; CT-26 cells, murine colon cancer cells; PBS, phosphate-buffered saline; NIR, near-infrared; DC, dendritic cell; CD, cluster of differentiation; MHC, major histocompatibility complex; IgG, immunoglobulin G, ANOVA, analysis of variance; SEM, standard error mean

Discussion

Various drug delivery systems are being developed for tumor treatment to suppress side effects and increase treatment efficiency [31]. Similar to COVID-19 vaccines, lipid-based nanoparticles are being developed as carriers for anticancer drugs and immunotherapies [32]. Lipid-based nanostructures are advantageous because they employ lipids similar to cellular membrane components; however, the side effects caused by PEGylation, which is used for stability, are problematic [32]. Therefore, in this study, natural polysaccharides were used as carriers to deliver drugs, as they offer biological activity without side effects [20]. Chitosan has low immunogenicity and is used as a material that can deliver various drugs by surface charge without causing side effects such as inflammation [20]. In addition, CFP has exhibited its potential as an immune stimulator by triggering the activity of DCs and natural killer (NK) cells in humans and mice [15, 17]. The combination of these two polysaccharides resulted in the formation of nanoparticles with appropriate size and characteristics for drug delivery. In addition, CC-ICG was used as a photoimmunotherapy agent to develop a

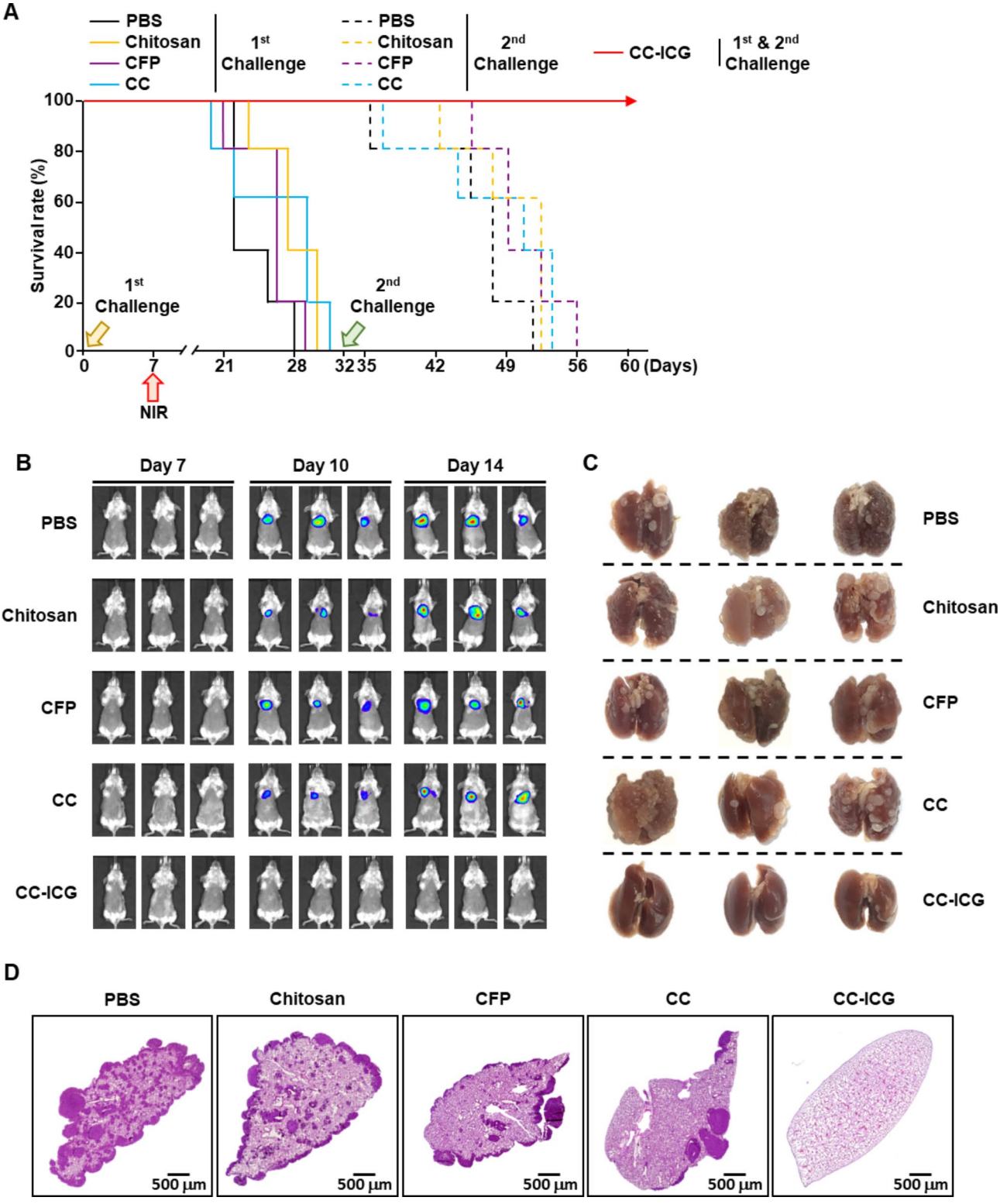

Fig. 5 CC-ICG-cured mice survived rechallenged lung metastatic CT-26 cancer On day 32 of primary CT-26 tumor injection, the CC-ICG-cured mice are rechallenged with CT-26-iRFP by *i.v.* injection. PBS, chitosan, CFP, and CC are administered to mice as the rechallenge controls. **(A)** Survival rate of mice after CT-26 tumor primary challenge and rechallenge of CT-26 tumors ($n = 5$). **(B)** The iRFP fluorescence of CT-26-iRFP on the indicated day of rechallenge is analyzed using an in vivo imaging system. **(C)** Representative photographs of lung tissues on day 14 of the CT-26-iRFP rechallenge. **(D)** Hematoxylin and eosin staining of lung tissues. Data are representative of analyses from six independent samples ($n = 6$, two-way ANOVA, mean ± SEM, $^{**}p < 0.01$). CFP, *Codium fragile* polysaccharide; CC, chitosan-CFP; ICG, indocyanine green; CC-ICG, chitosan-CFP-ICG; PBS, phosphate-buffered saline; NIR, near-infrared; ANOVA, analysis of variance; SEM, standard error mean; *i.v.*, intravenous

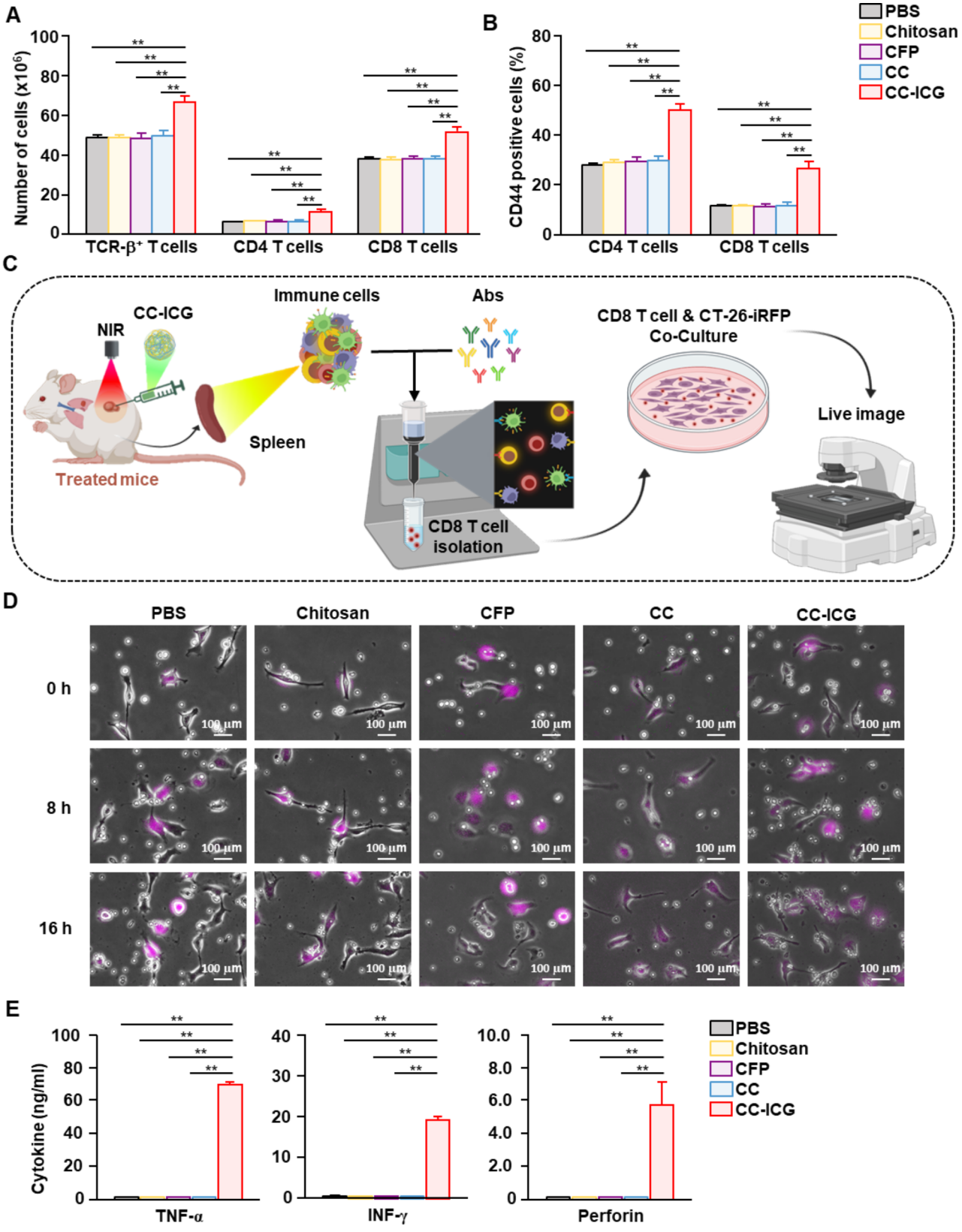

Fig. 6 (See legend on next page.)

(See figure on previous page.)

Fig. 6 CC-ICG-mediated PTT elicits memory immunity against CT-26 cells Splenocytes are harvested from mice on day 14 after CT-26-iRFP rechallenge. **(A)** Total number of TCR-β^+ T, CD4 T, and CD8 T cells in the spleen. **(B)** Percentage of $CD44^+$ memory cells in CD4 and CD8 T cells. **(C)** Schematic illustration of CTL activity evaluation by co-culture with CT-26-iRFP. **(D)** Time-dependent imaging of CTLs co-cultured with CT-26-iRFP. **(E)** Concentrations of indicated cytokines measured in the culture medium. Data are representative and averaged from six independent samples ($n = 6$, two-way ANOVA, mean ± SEM, $^{**}p < 0.01$). PTT, photothermal therapy; CFP, *Codium fragile* polysaccharide; CC, chitosan-CFP; ICG, indocyanine green; CC-ICG, chitosan-CFP-ICG; CT-26 cells, murine colon cancer cells; PBS, phosphate-buffered saline; NIR, near-infrared; TCR, T cell receptor; CD, cluster of differentiation; CTL, cytotoxic T lymphocyte; IFN, interferon; TNF, tumor necrosis factor

new nanomedicine that can treat primary tumors and prevent metastasis and recurrence.

Cancer immunotherapy utilizes the cytotoxic activity of CTLs and NK cells [9, 11]. Unlike NK cells, CTLs recognize antigens and exhibit selective cytotoxicity, leading to cancer cell death [9]. In this way, antigen recognition by CTLs is driven by antigen presentation by DCs. While CTL activity has been extensively studied in cancer immunotherapy using drug delivery systems, the role of DC activity has often been underreported [33–35]. Although in vitro-differentiated DCs originate from bone marrow cells, they often differ from in vivo DCs in terms of size, shape, and function [36, 37]. In addition, when DCs are activated by antigens in peripheral tissues or blood, they must migrate to the spleen or lymph nodes; however, these indicators cannot be confirmed in DCs differentiated in vitro [37, 38]. Therefore, research on CTL-mediated cancer immunotherapy requires in vivo data on the activity of DCs in the spleen or lymph nodes of mice [39–41]. In vivo DC activity in these organs directly supports the induction of CTL activity [39–41]. In this study, based on the DC activation capacity of CFP, we demonstrated that DCs in the spleen were activated after CC-ICG-mediated PTT. In addition, CC-ICG treatment increased the number of DCs in the spleen, indicating DCs from peripheral blood or tissue had migrated to the spleen. Therefore, these data suggest that splenic DCs are sufficiently activated by CC-ICG to induce CTL activity.

Immunotherapy studies to treat tumors in peripheral tissues must confirm the activity of lymph node immune cells [42, 43]. When studying immunotherapy in subcutaneously transplanted tumors, DC and T cell activity in the inguinal lymph nodes should be analyzed [43]. However, we analyzed the activation of DCs and T cells in the spleen. We did not confirm the results of immune activation in lymph nodes because the purpose of this study was to block tumor recurrence and metastasis after primary cancer treatment. For this purpose, we used a lung metastasis model in which lung metastasis was induced by intravenous administration. Pathogens administered systemically in this way are responsible for immunity in the spleen [44]. Therefore, we concluded that confirming immune activity in the spleen, which is responsible for systemic immunity, supports the development of a defense system against circulating cancer cells.

PTT has a great advantage in that it only affects the area irradiated by the laser [21]. For tumors located close to the skin, such as skin cancer or breast cancer, PTT is efficient for treatment [21, 45]. However, this localized effect can be a disadvantage when treating tumors in internal organs that cannot be directly reached by the laser. To overcome these limitations, methods involving wavelengths with deeper tissue penetration or the use of laser irradiation following open surgery can be employed [21, 46]. The ICG used in this study induces a temperature-increasing effect in response to the NIR laser, but its transmittance is low due to its high wavelength [46]. Therefore, applying laser irradiation after laparotomy for internal organ tumors are appropriate.

Nanoparticles are advantageous because they target specific tumors [47, 48]. Antibodies or ligands that act as active targets are bound to the surface of the nanoparticle [49], and passive targeting relies on the enhanced permeability and retention (EPR) effect by controlling nanoparticle size [50]. However, the tumor-targeting efficiency of nanoparticles is not satisfactory under passive or active target conditions [47, 51]. In this study, we aimed to use the EPR effect for PTT, but owing to the limit of the amount of CC-ICG delivered inside the tumor, a sufficient temperature increase could not be achieved even with NIR laser irradiation. In subsequent studies, we will focus on ways to improve the tumor-targeting efficiency of nanoparticles to enhance the effectiveness of photoimmunotherapy for the treatment of primary tumors and prevention of their metastasis and recurrence.

Conclusions

In conclusion, we synthesized ICG-loaded nanoparticles using the respective charge combinations of chitosan and CFP. CC-ICG-mediated PTT showed a thermal-raising effect with the NIR laser and induced complete tumor remission. In addition, the immune response induced by CC-ICG while treating the primary tumor suppressed the growth of re-administered lung metastasis cancer. Therefore, the CC-ICG nanoparticles developed in this study is a promising novel nanomedicine for treating primary cancer and preventing metastasis and recurrence via photoimmunotherapy.

Abbreviations

CFP	Codium fragile polysaccharide
CC-ICG	Chitosan/CFP-indocyanine green
CT-26 cells	Murine colon cancer cells

CTL	Cytotoxic T lymphocyte
DC	Dendritic cell
PTT	Photothermal therapy
NIR	Near-infrared
CC	Chitosan-CFP
TEM	Transmission electron microscopy
FBS	Fetal bovine serum
CT-26-iRFP cells	CT-26WT-iRFP-Neo cells
PBS	Phosphate-buffered saline
DAPI	4′,6-diamidino-2-phenylindole
CD	Cluster of differentiation
FITC	Fluorescein isothiocyanate
APC	Allophycocyanin
PE	Phycoerythrin
PerCP	Peridinin-chlorophyll-protein
TCR	T cell receptor
BM	Bone marrow
BMDC	Bone marrow-derived dendrite cells
MHC	Major histocompatibility complex
i.v.	intravenously
iRFP	Near-infrared fluorescent protein
H&E	Hematoxylin and eosin
EPR	Enhanced permeability and retention

Supplementary Information

The online version contains supplementary material available at https://doi.org/10.1186/s12951-024-02944-0.

Supplementary Material 1

Supplementary Material 2

Supplementary Material 3

Supplementary Material 4

Supplementary Material 5

Supplementary Material 6

Acknowledgements
We thank the Asan Medical Center animal facility for maintaining the animals used in this study. In addition, we thank the Asan Life Science Research Institute for providing the Litesizer™ 500 to measure particle size and zeta potential.

Author contributions
Dayoung Ryu and Hae-Bin Park: Investigation, Methodology, Validation. Eun-Koung An and So-Jung Kim: Data curation, Formal analysis, Visualization. Da young Kim, Daeun Lim and Juyoung Hwang: Formal analysis. Minseok Kwak, Wonpil Im, and Ja-Hyoung Ryu: Conceptualization, Formal analysis, Methodology, Supervision, Writing–review and editing. Jun-O Jin, SangGuan You and Peter C.W. Lee: Conceptualization, Funding acquisition, Project administration, Supervision, Writing–review and editing.

Funding
This study was supported by the Basic Research Program through the National Research Foundation of Korea, funded by MSIT (RS-2023-00207868 and RS-2023-00281553). Moreover, this study was also supported by a Asan Medical Center grant (2023IP0126).

Data availability
No datasets were generated or analysed during the current study.

Declarations

Ethics approval and consent to participate
Not applicable.

Consent for publication
Not applicable.

Competing interests
The authors declare no competing interests.

Received: 17 July 2024 / Accepted: 20 October 2024
Published online: 23 October 2024

References

1. Leiter A, Veluswamy RR, Wisnivesky JP. The global burden of lung cancer: current status and future trends. Nat Reviews Clin Oncol. 2023;20:624–39.
2. Li J, Wang S, Fontana F, Tapeinos C, Shahbazi M-A, Han H, Santos HA. Nanoparticles-based phototherapy systems for cancer treatment: current status and clinical potential. Bioactive Mater. 2023;23:471–507.
3. Naito Y, Nishida T, Doi T. Current status of and future prospects for the treatment of unresectable or metastatic gastrointestinal stromal tumours. Gastric Cancer. 2023;26:339–51.
4. Manzanedo I, Pereira F, Pérez-Viejo E, Serrano Á. Gastric Cancer with peritoneal metastases: current status and prospects for treatment. Cancers. 2023;15:1777.
5. Gerstberger S, Jiang Q, Ganesh K. Metastasis. Cell. 2023;186:1564–79.
6. Diamantopoulou Z, Gvozdenovic A, Aceto N. A new time dimension in the fight against metastasis. Trends Cell Biol. 2023;33:736–48.
7. Peri A, Salomon N, Wolf Y, Kreiter S, Diken M, Samuels Y. The landscape of T cell antigens for cancer immunotherapy. Nat cancer. 2023;4:937–54.
8. Schaft N, Dörrie J, Schuler G, Schuler-Thurner B, Sallam H, Klein S, Eisenberg G, Frankenburg S, Lotem M, Khatib A. The future of affordable cancer immunotherapy. Front Immunol. 2023;14:1248867.
9. Oliveira G, Wu CJ. Dynamics and specificities of T cells in cancer immunotherapy. Nat Rev Cancer. 2023;23:295–316.
10. Najafi S, Mortezaee K. Advances in dendritic cell vaccination therapy of cancer. Biomed Pharmacother. 2023;164:114954.
11. Del Prete A, Salvi V, Soriani A, Laffranchi M, Sozio F, Bosisio D, Sozzani S. Dendritic cell subsets in cancer immunity and tumor antigen sensing. Cell Mol Immunol. 2023;20:432–47.
12. Zhang W, Xu L, Park H-B, Hwang J, Kwak M, Lee PC, Liang G, Zhang X, Xu J, Jin J-O. Escherichia coli adhesion portion FimH functions as an adjuvant for cancer immunotherapy. Nat Commun. 2020;11:1187.
13. Tang C, Ding R, Sun J, Liu J, Kan J, Jin C. The impacts of natural polysaccharides on intestinal microbiota and immune responses–a review. Food Funct. 2019;10:2290–312.
14. Jin J-O, Yadav D, Madhwani K, Puranik N, Chavda V, Song M. Seaweeds in the oncology arena: anti-cancer potential of fucoidan as a drug—A review. Molecules. 2022;27:6032.
15. Park H-B, Lim S-M, Hwang J, Zhang W, You S, Jin J-O. Cancer immunotherapy using a polysaccharide from Codium fragile in a murine model. Oncoimmunology. 2020;9:1772663.
16. Yang Y, Park J, You SG, Hong S. Immuno-stimulatory effects of sulfated polysaccharides isolated from Codium fragile in olive flounder, Paralichthys olivaceus. Fish Shellfish Immunol. 2019;87:609–14.
17. Park H-B, Hwang J, Zhang W, Go S, Kim J, Choi I, You S, Jin J-O. Polysaccharide from Codium fragile induces anti-cancer immunity by activating natural killer cells. Mar Drugs. 2020;18:626.
18. Kou SG, Peters LM, Mucalo MR. Chitosan: a review of sources and preparation methods. Int J Biol Macromol. 2021;169:85–94.
19. Aranaz I, Alcántara AR, Civera MC, Arias C, Elorza B, Heras Caballero A, Acosta N. Chitosan: an overview of its properties and applications. Polymers. 2021;13:3256.
20. Wang J, Zhuang S. Chitosan-based materials: Preparation, modification and application. J Clean Prod. 2022;355:131825.
21. Zhi D, Yang T, O'hagan J, Zhang S, Donnelly RF. Photothermal therapy. J Controlled Release. 2020;325:52–71.
22. Lan M, Zhao S, Liu W, Lee CS, Zhang W, Wang P. Photosensitizers for photodynamic therapy. Adv Healthc Mater. 2019;8:1900132.
23. Li Y, Cui J, Li C, Deng C, Deng G, Zhang H, An F. Biomaterial-assisted photoimmunotherapy for synergistic suppression of cancer progression. Chin Chem Lett. 2023;34:108180.
24. Nasseri B, Alizadeh E, Bani F, Davaran S, Akbarzadeh A, Rabiee N, Bahadori A, Ziaei M, Bagherzadeh M, Saeb MR. Nanomaterials for photothermal and photodynamic cancer therapy. Appl Phys Reviews 2022, 9.

25. Tabarsa M, Karnjanapratum S, Cho M, Kim J-K, You S. Molecular characteristics and biological activities of anionic macromolecules from Codium fragile. Int J Biol Macromol. 2013;59:1–12.
26. Wang Y, An E-K, Kim S-J, You S, Jin J-O. Intranasal administration of Codium fragile polysaccharide elicits anti-cancer immunity against Lewis lung carcinoma. Int J Mol Sci. 2021;22:10608.
27. Kim S-J, Park H-B, An E-K, Ryu D, Zhang W, Pack C-G, Kim H, Kwak M, Im W, Ryu J-H. Lipid-coated gold nanorods for photoimmunotherapy of primary breast cancer and the prevention of metastasis. J Controlled Release. 2024;373:105–16.
28. Kim SJ, Park HB, An EK, Eom HY, Zhang W, Kim J, Choi I, Kwak M, Lee PC, Jin JO. Artificial Immunogenic cell death lipid nanoparticle functions as a therapeutic vaccine for Cancer. Adv Funct Mater. 2023;33:2302825.
29. Coutinho AJ, Lima SAC, Afonso CM, Reis S. Mucoadhesive and pH responsive fucoidan-chitosan nanoparticles for the oral delivery of methotrexate. Int J Biol Macromol. 2020;158:180–8.
30. Zhang W, Hwang J, Park H-B, Lim S-M, Go S, Kim J, Choi I, You S, Jin J-O. Human peripheral blood dendritic cell and T cell activation by Codium fragile polysaccharide. Mar Drugs. 2020;18:535.
31. Ezike TC, Okpala US, Onoja UL, Nwike PC, Ezeako EC, Okpara JO, Okoroafor CC, Eze SC, Kalu OL, Odoh EC. Advances in drug delivery systems, challenges and future directions. *Heliyon* 2023.
32. Hao Y, Ji Z, Zhou H, Wu D, Gu Z, Wang D, Ten Dijke P. Lipid-based nanoparticles as drug delivery systems for cancer immunotherapy. MedComm. 2023;4:e339.
33. Han J, Lim J, Wang C-PJ, Han J-H, Shin HE, Kim S-N, Jeong D, Lee SH, Chun B-H, Park CG. Lipid nanoparticle-based mRNA delivery systems for cancer immunotherapy. Nano Convergence. 2023;10:36.
34. Zhang Y, Chen J, Shi L, Ma F. Polymeric nanoparticle-based nanovaccines for cancer immunotherapy. Mater Horiz. 2023;10:361–92.
35. Hu Y, Zhang W, Chu X, Wang A, He Z, Si C-L, Hu W. Dendritic cell-targeting polymer nanoparticle-based immunotherapy for cancer: a review. Int J Pharm. 2023;635:122703.
36. Mittag D, Proietto AI, Loudovaris T, Mannering SI, Vremec D, Shortman K, Wu L, Harrison LC. Human dendritic cell subsets from spleen and blood are similar in phenotype and function but modified by donor health status. J Immunol. 2011;186:6207–17.
37. Naik SH, Sathe P, Park H-Y, Metcalf D, Proietto AI, Dakic A, Carotta S, O'Keeffe M, Bahlo M, Papenfuss A. Development of plasmacytoid and conventional dendritic cell subtypes from single precursor cells derived in vitro and in vivo. Nat Immunol. 2007;8:1217–26.
38. Garrigan K, Moroni-Rawson P, McMurray C, Hermans I, Abernethy N, Watson J, Ronchese F. Functional comparison of spleen dendritic cells and dendritic cells cultured in vitro from bone marrow precursors. 1996.
39. Vremec D, Pooley J, Hochrein H, Wu L, Shortman K. CD4 and CD8 expression by dendritic cell subtypes in mouse thymus and spleen. J Immunol. 2000;164:2978–86.
40. Lewis SM, Williams A, Eisenbarth SC. Structure and function of the immune system in the spleen. Sci Immunol. 2019;4:eaau6085.
41. Naik SH, Proietto AI, Wilson NS, Dakic A, Schnorrer P, Fuchsberger M, Lahoud MH, O'Keeffe M, Shao Q-x. Chen W-f: cutting edge: generation of splenic CD8 + and CD8 – dendritic cell equivalents in Fms-like tyrosine kinase 3 ligand bone marrow cultures. J Immunol. 2005;174:6592–7.
42. Yoshizawa H, Chang AE, Shu S. Specific adoptive immunotherapy mediated by tumor-draining lymph node cells sequentially activated with anti-CD3 and IL-2. *Journal of immunology (Baltimore, Md*: 1950) 1991, 147:729–737.
43. Van Pul KM, Fransen MF, Van de Ven R, De Gruijl TD. Immunotherapy goes local: the central role of lymph nodes in driving tumor infiltration and efficacy. Front Immunol. 2021;12:643291.
44. Kashimura M. The human spleen as the center of the blood defense system. Int J Hematol. 2020;112:147–58.
45. Alamdari SG, Amini M, Jalilzadeh N, Baradaran B, Mohammadzadeh R, Mokhtarzadeh A, Oroojalian F. Recent advances in nanoparticle-based photothermal therapy for breast cancer. J Controlled Release. 2022;349:269–303.
46. Chu Y, Xu X-Q, Wang Y. Ultradeep photothermal therapy strategies. J Phys Chem Lett. 2022;13:9564–72.
47. Thakkar S, Sharma D, Kalia K, Tekade RK. Tumor microenvironment targeted nanotherapeutics for cancer therapy and diagnosis: a review. Acta Biomater. 2020;101:43–68.
48. Ryu JH, Yoon HY, Sun IC, Kwon IC, Kim K. Tumor-targeting glycol chitosan nanoparticles for cancer heterogeneity. Adv Mater. 2020;32:2002197.
49. Marques A, Costa P, Velho S, Amaral M. Functionalizing nanoparticles with cancer-targeting antibodies: a comparison of strategies. J Controlled Release. 2020;320:180–200.
50. Shinde VR, Revi N, Murugappan S, Singh SP, Rengan AK. Enhanced permeability and retention effect: a key facilitator for solid tumor targeting by nanoparticles. Photodiagn Photodyn Ther. 2022;39:102915.
51. Niculescu A-G, Grumezescu AM. Novel tumor-targeting nanoparticles for cancer treatment—A review. Int J Mol Sci. 2022;23:5253.

Publisher's note